Localized Lorenz Energy Cycle Reveals a New Scenario of Multiscale Interaction Underlying the Winter North Atlantic Oscillation

JIWANG MA[a,b] AND X. SAN LIANG[b,a,c]

[a] *The Artificial Intelligence Department, Division of Frontier Research, Southern Marine Science and Engineering Guangdong Laboratory (Zhuhai), Zhuhai, China*
[b] *CMA–FDU Joint Laboratory of Marine Meteorology, Department of Atmospheric and Oceanic Sciences, Fudan University, Shanghai, China*
[c] *IRDR ICoE on Risk Interconnectivity and Governance on Weather/Climate Extremes Impact and Public Health, Fudan University, Shanghai, China*

(Manuscript received 25 September 2024, in final form 22 April 2025, accepted 6 May 2025)

ABSTRACT: Lying at the heart of the North Atlantic Oscillation (NAO) is the interaction between the low-frequency processes and synoptic eddies. Though extensively studied, a consensus is still elusive. Particularly, a localized Lorenz energy cycle is lacked, which may provide a scenario with details disappearing in the global cycles as obtained. Using a functional analysis apparatus specifically for this purpose, namely, multiscale window transform (MWT), and the MWT-based theory of canonical transfer, for the first time such a cycle is constructed here. The result clearly shows that the energetic processes occur in different regions—a characteristic overlooked in previous studies. Specifically, we find that the kinetic energy (KE) transferred from the synoptic eddies to the low-frequency flow (over the ocean southwest of the British Isles) is first transported to the rising branch of the secondary circulation at the exit region of the NAO jet stream and converted into available potential energy (APE) there. The gained APE is then transported to the sinking branch of the secondary circulation at the entrance region of the jet stream, enhancing its ambient baroclinicity. More synoptic eddies are hence generated, and their energy is transported to the southwest of the British Isles to compensate the energy consumption there. These processes together form a localized energy loop, in which the low-frequency flow and the synoptic eddies feed each other, generating a positive feedback. The implications here are that the positive feedback mechanism proposed in a zonally uniform framework with only one secondary circulation may need to be updated to incorporate two secondary circulations, together with their localized spatial variations.

KEYWORDS: Feedback; Energy budget/balance; North Atlantic Oscillation; Instability; Storm tracks; Synoptic-scale processes

1. Introduction

North Atlantic Oscillation (NAO) is the dominant low-frequency mode over the Northern Hemisphere. It has substantial influences on the ambient and remote weather and climate (e.g., Barnes et al. 2019; Hurrell and Deser 2009; Kenyon and Hegerl 2008), and its variabilities have a close relationship with global warming (Cohen and Barlow 2005; Hurrell 1995, 1996). For these reasons, among others, much effort has been devoted to understanding what is underlying its genesis and maintenance.

Interactions between the low-frequency processes and synoptic eddies are found to be essential to NAO dynamics. Particularly, a positive feedback is emphasized in many studies, such as, on an incomplete list, Barnes et al. (2010), Barnes and Hartmann (2010), Cai and Mak (1990), Feldstein and Lee (1998), Jin et al. (2006a,b), Jin (2010), Kug and Jin (2009), Limpasuvan and Hartmann (1999), Lorenz and Hartmann (2001), Luo et al. (2007a,b, 2015), Ren et al. (2009, 2012), Robinson (1991, 1996, 2000, 2006), Song (2016), and Zhang et al. (2012). Among these studies, the positive feedback is investigated from different perspectives. Jin et al. (2006a,b) propose a linear closure relating the ensemble-mean eddy forcing and time-mean flows in a semianalytical study. The study is based on a stochastic basic flow, which captures the climatological mean flow and climatological statistics of the synoptic eddies, and hence is closely related to the real atmosphere. In their study, NAO is found to be the leading eigenmode of a linear system. An eddy-induced instability is further proposed to qualitatively explain the mechanisms underlying the interactions between synoptic eddies and the low-frequency flow, and a "left-hand rule" is concepted to facilitate the analysis of the eddy-vorticity fluxes in amplifying the flow (Jin 2010; Kug and Jin 2009). On the other hand, after investigating the interactions between the synoptic-scale and planetary-scale waves, Luo et al. (2005, 2015, 2007a) show that NAO is actually an initial-value problem in their highly idealized multiscale model. In the model, specific synoptic-scale waves and a planetary-scale wave with a dipole structure are prespecified as the initial condition of the model. They find that the positive feedback holds only when the preexisting synoptic eddy forcing matches the dipole structure of planetary waves. It should be mentioned that the above two studies include only the barotropic processes. Robinson (1996, 2000, 2006) takes into account baroclinic processes in his studies and finds that, with a simple circulation model, they are crucial in the positive feedback between the low-frequency components and synoptic eddies. The low-frequency circulation is believed to be important in enhancing the baroclinicity where eddies generate. Then, the eddies propagate away,

Corresponding author: X. San Liang, xsliang@fudan.edu.cn

DOI: 10.1175/JAS-D-24-0210.1

break, and are dissipated to strengthen the low-frequency circulation due to the convergence of the Eliassen–Palm flux. As a result, the low-frequency circulation and eddies fuel each other and form a positive feedback. Lorenz and Hartmann (2003) also find a critical role in the positive feedback in their diagnostic study. Barnes and Hartmann (2010) further include the adiabatic cooling mechanism in the positive feedback.

From above, it is clear that the conceptual model of positive feedback is critical in aiding to understand the dynamics of NAO and other low-frequency processes. However, it is still too early to say that the positive feedback is fully understood. Particularly, the diagnostics of the interaction between the low-frequency and synoptic eddies underlying NAO from the perspective of localized energetics are yet to be investigated. In this regard, Castanheira and Marques (2019) conduct a study of energy cascade in a global-mean manner. Unfortunately, NAO is a localized phenomenon, and hence, a global-mean energetics may involve processes out of the NAO zone. In this sense, a localized Lorenz energy cycle is desired. It is well known that the Lorenz energy cycle is initially designed in a global framework. Releasing it from a global form to a localized one is actually by no means an easy task. Thanks to a new mathematical apparatus, namely, multiscale window transform (MWT), and the systematic work on localized multiscale energetics and canonical transfer during the past decades (refer to section 2 for details), the localized Lorenz energy cycle of NAO will be constructed for the first time to deepen the understanding of its dynamics. Another merit distinguishing this study from other previous NAO (or NAO like) studies is that the low-frequency processes are variable in time since they are reconstructed through MWT (like filtering), not temporally invariant climatology means as adopted in previous studies (e.g., Simmons et al. 1983; Tanaka et al. 2016; Martineau et al. 2020; Zhuge and Tan 2021; Wang and Tan 2021; Sun et al. 2021; Kim et al. 2021, 2024). This fact allows us to deal with the NAO low-frequency modulation on the interactions of the basic flow and synoptic eddies.

2. Data and method

a. Data

The datasets used in this study are the NAO index from the Climate Prediction Center of National Oceanic and Atmospheric Administration (Barnston and Livezey 1987) and the ERA-40 (https://apps-dev.ecmwf.int/datasets/data/era40-daily/levtype=pl/) dataset from the European Centre for Medium-Range Weather Forecasts (ECMWF) (Uppala et al. 2005). Temperature (T), wind velocity components (u, v, ω), and geopotential (Φ) in the ERA dataset are involved in the calculation. It has a time resolution of 6 h and a spatial resolution of 2.5° × 2.5°, covering the zonal circle between 30° and 85°N horizontally and from 1000 to 50 hPa vertically. A period with 2^{16} time steps, starting 1 September 1957 and ending 21 May 2002, is chosen, since the length with a power of 2 time steps is required by the analysis methodology (see below). The results in this study are also verified using the ERA5 dataset (https://cds.climate.copernicus.eu/datasets/reanalysis-era5-pressure-levels?tab=download) (Hersbach et al. 2020). Its time span covers the first half of that with the ERA-40 dataset. They are consistent with the results here based on ERA-40 (not shown). These facts mean that the results are robust and insensitive to datasets and time spans.

b. Multiscale window transform, multiscale energetics analysis, and canonical transfer

1) Multiscale window transform

For the purpose of multiscale geophysical fluid dynamics studies, Liang and Anderson (2007) developed a functional analysis apparatus called MWT. In orthogonally decomposing a field by scale to provide filtered fields (reconstructions), MWT simultaneously provides a transform coefficient for each filtered field. The orthogonality ensures energy conservation during a decomposition (thanks to the Parseval relation in functional analysis), while the transform coefficients make it possible to express multiscale energies in terms of them. This is in contrast to most of the widely used filters; they do not have transform coefficients and hence actually cannot have this multiscale energy representation. Notice that, in the literature, a common practice is to simply take the square of a filtered field as the corresponding multiscale energy. Unfortunately, this is wrong even in concept. For example, consider an even function $f(t)$. In its Fourier power spectrum, if corresponding to a frequency ω is the Fourier coefficient $\widehat{a}$, then the energy on the time scale of $2\pi/\omega$ is $\widehat{a}^2$. It is a concept in phase space. In the meantime, the square of the reconstruction is $[\widehat{a}\cos(\omega t)]^2$. Obviously, it is not equal to $\widehat{a}^2$, and, moreover, it is a concept in physical space (a function of t), conceptually different from the multiscale energy.

In MWT, a function space is decomposed into subspaces called scale windows, which exclusively span a range of scales. In this study, we will need a low-frequency window where lies the NAO signal (or simply NAO window if no confusion may arise in the context) and a high-frequency (or synoptic) window. For convenience, these windows are denoted as 0 and 1, respectively. In this study, the MWT of a field, say T, is symbolically written as $\widehat{T}_n^{\sim\varpi}$, where n is the time step and $\varpi = 0, 1$ denotes the scale window. The corresponding reconstructions, i.e., filtered fields, are accordingly written as $T_n^{\sim\varpi}$.

A comprehensive introduction of MWT is beyond the scope of this study. The reader is referred to Liang and Anderson (2007) for details. A more readable short introduction can be seen in Liang (2016).

2) Canonical transfer

Multiscale energetics analysis has become a powerful tool for investigating the dynamical processes underlying geophysical fluid flow, thanks to Lorenz's (1955) seminal work. Lorenz's formalism, however, is in an integral/average form, lacking the needed local information for most of the weather and climate processes. In the literature, many studies attempt to get around this difficulty by simply removing the average operators. It seems to be effective but, unfortunately, is conceptually misleading. As elaborated in Liang (2016) and many other publications that removing the average operator from the eddy energy formula with a Reynolds decomposition does not yield the "localized eddy energy," in fact, it is not at all energy in the

physical sense. The average operator ensures a connection of the so-obtained eddy energy to the eddy energy in the phase space through the renowned Parseval identity in functional analysis; otherwise, the so-obtained "energy" would not be conserved.

On the other hand, localizing the bulk Lorenz formalism is faced with an obstacle on how to separate the cross-scale transfer from in-scale transport, which is rather subjective in classical formalisms and not unique. This is a rather fundamental problem [as identified in some early pioneering studies such as Plumb (1983)] which, however, has been mostly overlooked. Liang and Robinson (2005, 2007), tackle this systematically for the first time, using the aforementioned MWT as the machinery. The thus-obtained transfer is proved to be unique by Liang (2016), bears a Lie bracket form, which is like the Poisson bracket in Hamiltonian dynamics, and satisfies the Jacobian identity, among many other properties. Accordingly, it has been termed a canonical transfer. In the following, we simply write out the formula for computation; the reader is referred to Liang (2016) for details.

The multiscale kinetic energy (KE) and available potential energy (APE) equations are (Liang 2016)

$$\frac{\partial K^{\varpi}}{\partial t}+\underbrace{\nabla\cdot\left[\frac{1}{2}\widehat{(\mathbf{v}\mathbf{v}_h)}^{\sim\varpi}\cdot\hat{\mathbf{v}}_h^{\sim\varpi}\right]}_{\nabla\cdot\mathbf{Q}_K^{\varpi}}=\underbrace{\frac{1}{2}\left\{\widehat{(\mathbf{v}\mathbf{v}_h)}^{\sim\varpi}:\nabla\hat{\mathbf{v}}_h^{\sim\varpi}-[\nabla\cdot\widehat{(\mathbf{v}\mathbf{v}_h)}^{\sim\varpi}]\cdot\hat{\mathbf{v}}_h^{\sim\varpi}\right\}}_{\Gamma_K^{\varpi}}-\underbrace{\nabla\cdot(\hat{\mathbf{v}}^{\sim\varpi}\widehat{\Phi}^{\sim\varpi})}_{\nabla\cdot\mathbf{Q}_P^{\varpi}}-\underbrace{\widehat{\omega}^{\sim\varpi}\widehat{\alpha}^{\sim\varpi}}_{b^{\varpi}}+F_K^{\varpi}, \tag{1}$$

$$\frac{\partial A^{\varpi}}{\partial t}+\underbrace{\nabla\cdot\left[\frac{1}{2}c\widehat{(\mathbf{v}T)}^{\sim\varpi}\widehat{T}^{\sim\varpi}\right]}_{\nabla\cdot\mathbf{Q}_A^{\varpi}}=\underbrace{\frac{c}{2}[\widehat{(\mathbf{v}T)}^{\sim\varpi}\cdot\nabla\widehat{T}^{\sim\varpi}-\widehat{T}^{\sim\varpi}\nabla\cdot\widehat{(\mathbf{v}T)}^{\sim\varpi}]}_{\Gamma_A^{\varpi}}+\underbrace{\widehat{\omega}^{\sim\varpi}\widehat{\alpha}^{\sim\varpi}}_{b^{\varpi}}+F_A^{\varpi}, \tag{2}$$

where K^{ϖ} and A^{ϖ} denote the KE and APE on window ϖ, $\mathbf{v}_h$ means the horizontal component of velocity, ω is the vertical velocity, Φ is the geopotential, T is the temperature, and α is the specific volume. The symbol "$\widehat{\ }^{\sim\varpi}$" is the MWT transform coefficient on scale window ϖ. Note here there should be a subscript n indicating the location, but for simplicity, it has been suppressed. The operator "**:**" in Eq. (1) is defined, for vectors **A**, **B**, **C**, and **D**, as (**AB**):(**CD**) = (**A** · **C**)(**B** · **D**). Other symbols are conventional. The terms $\nabla\cdot\mathbf{Q}_K$, $\nabla\cdot\mathbf{Q}_P$, Γ_K, b, and F_K represent KE transport, pressure work, KE canonical transfer among scales, buoyancy conversion, and dissipation, respectively. This transfer Γ has a nice property $\sum_{\varpi}\sum_n\Gamma_n^{\varpi}=0$, which means that this kind of process only redistributes energy among scales; it does not generate nor destroy energy as a whole; in other words, it ensures energy conservation, in contrast to the traditional counterparts.

MWT and the MWT-based multiscale energetics analysis have been validated with benchmark geophysical fluid dynamical processes (e.g., Liang and Robinson 2007) and applied successfully to many real atmosphere–ocean–climate problems. The most recent ones include those on stratospheric sudden warming (Xu and Liang 2017), atmospheric blocking (Ma and Liang 2017, 2023a), storm track (Zhao et al. 2019), cold wave outbreak (Xu and Liang 2020), Gulf of Mexico circulation (Yang et al. 2020, 2021), squall line (Guo and Liang 2022), tropical cyclone (Song et al. 2023), and Madden–Julian oscillation (Ma et al. 2023), to name a few.

3) PROJECTION ONTO THE NAO INDEX

A variable, say, VAR, is projected onto the NAO index in the following way:

$$\mathrm{VAR}_p=\overline{\mathrm{VAR}(t)\times I(t)}, \tag{3}$$

where t represents time, the overbar means averaging, and I is the NAO index. Here, VAR refers to all the variables as examined in this study, including the energetics in Eqs. (1) and (2) as shown in Figs. 1–3, the geopotential in Figs. 1–4, and the vertical and zonal velocities in Fig. 4 in the following sections. Note that all the VARs are anomalies from their respective climatologies.

3. Localized Lorenz energy cycle

In this study, we focus on the interactions between high-frequency synoptic eddies and low-frequency processes (including time-mean flow) during the NAO. A two-scale separation framework is hence adopted here. That is to say, we will have the high-frequency and the low-frequency processes separated, with the synoptic eddies in the high-frequency scale window and the remaining in the low-frequency scale window. Using MWT as a filter, the original fields are separated into subfields on the low-frequency window (above 8 days) and high-frequency window (less than 8 days); more than a filter, also obtained are their corresponding MWT transform coefficients, which allow the energetics evaluated according to Eqs. (1) and (2). Again, a power of 2 is required by MWT for the number of time steps of the series. To test the sensitivity of the findings here to the window bound separating the low-frequency and high-frequency processes, we also adopt a 16-day window bound, redo all the analyses, and find that the results are consistent with that based on an 8-day window bound.

The required resulting variables for the analysis are then projected onto the NAO index. Frequently, one may see that some processes of NAO and the corresponding climatological ones are similar. As pointed out by Hansen and Sutera (1984) and Kushnir (1987), among others, these processes are misleading and cannot be used for the explanation of NAO

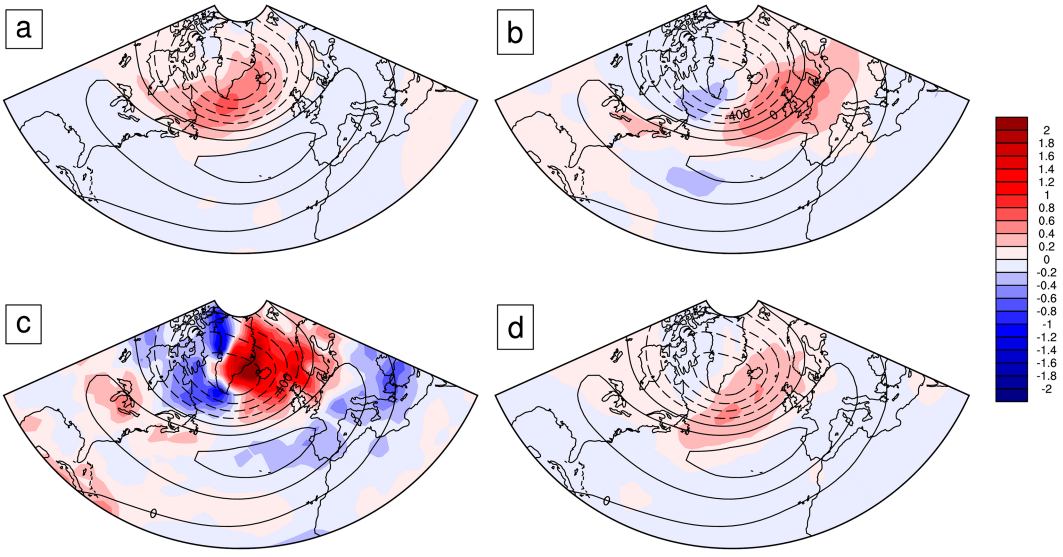

FIG. 1. The fields of baroclinic/barotropic transfers and buoyancy conversion superimposed with geopotential. The contoured are geopotential anomalies from the climatology projected onto the NAO index at 500 hPa ($m^2\ s^{-2}$). The shaded are (a) APE transfer from the low-frequency window to the high-frequency window ($\Gamma_A^{0\to1}$; $10^{-3}\ m^2\ s^{-3}$), (b) KE transfer from the high-frequency window to the low-frequency window ($\Gamma_K^{1\to0}$; $10^{-3}\ m^2\ s^{-3}$), (c) buoyancy conversion from KE to APE on the low-frequency window (b^0; $10^{-3}\ m^2\ s^{-3}$), and (d) buoyancy conversion from APE to KE on the high-frequency window ($-b^1$; $10^{-3}\ m^2\ s^{-3}$) anomalies from their respective climatologies projected onto the NAO index averaged from 500 hPa through 200 hPa. All the projections are fulfilled with Eq. (3).

development. We hence will only analyze the energetics anomalous to their climatology. Note that the climatological flow is NOT excluded in this study. It is actually the climatological energetics excluded. They are totally different. If the climatological flow were excluded, then the interactions of the flow and eddies would be missing; in the case with climatological energetics excluded, the interactions are kept, though they are anomalies. We are doing this for the purpose of visual clarity. For reference convenience, we will still refer to the anomalies as themselves, such as KE canonical transfers; that is to say, from now on, the KE canonical transfers should be understood as KE canonical transfers with their respective climatologies removed. In this sense, $A^{\varpi} > 0$ means that the APE on the ϖ window is greater than its climatology, likewise for other energetics processes. The energetics are then averaged through the upper troposphere from 500 to 200 hPa. This choice is made because the multiscale interactions in the lower troposphere and the upper troposphere are different (e.g., Hoskins et al. 1983; Lau and Nath 1991) so does the localized Lorenz energy cycle. As a result, adding these two kinds of energy cycle scenarios together (integrating through the whole troposphere) could blur their respective features and hence result in something misleading. Recall that our main finding in this work is the positive feedback from a perspective of energetics in the upper troposphere during NAO; we hence discuss the localized Lorenz energy cycle in the upper and lower tropospheres separately, with an emphasis on the upper one (the results in the lower troposphere are shown

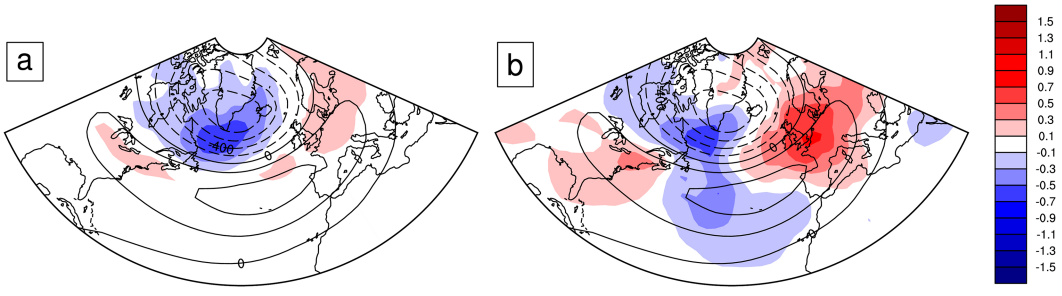

FIG. 2. High-frequency energy spatial redistribution. The contoured are geopotential anomalies from the climatology projected onto the NAO index at 500 hPa ($m^2\ s^{-2}$). The shaded are (a) APE transport on the high-frequency window ($-\nabla\cdot\mathbf{Q}_A^1$; $10^{-3}\ m^2\ s^{-3}$) and (b) KE transport and pressure work on the high-frequency window ($-\nabla\cdot\mathbf{Q}_K^1 - \nabla\cdot\mathbf{Q}_P^1$; $10^{-3}\ m^2\ s^{-3}$) anomalies to their climatology projected onto the NAO index averaged from 500 hPa through 200 hPa. All the projections are fulfilled with Eq. (3).

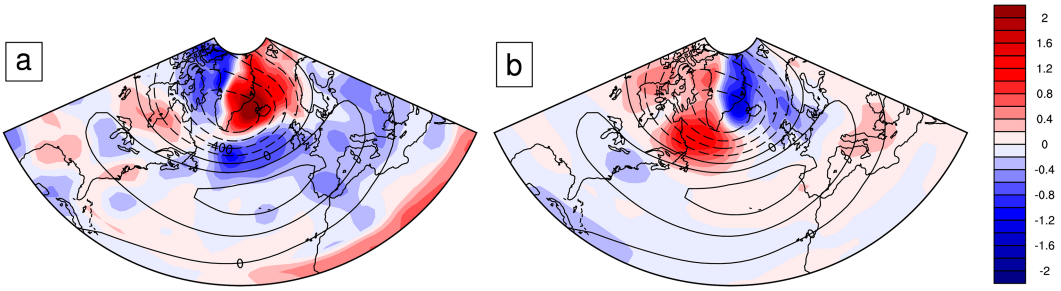

FIG. 3. Low-frequency energy spatial redistribution. Superimposed are the geopotential anomalies to their climatology projected onto the NAO index at 500 hPa (contoured; $m^2\ s^{-2}$). The shaded are (a) KE transport and pressure work on the low-frequency window ($-\nabla\cdot\mathbf{Q}_K^0 - \nabla\cdot\mathbf{Q}_K^0$; $10^{-3}\ m^2\ s^{-3}$) and (b) APE transport on the low-frequency window ($-\nabla\cdot\mathbf{Q}_A^0$; $10^{-3}\ m^2\ s^{-3}$) anomalies from their respective climatologies projected onto the NAO index averaged from 500 hPa through 200 hPa. All the projections are fulfilled with Eq. (3).

in appendix A for comparison). We note that the dynamics are asymmetric during NAO-positive (NAO+) and NAO-negative (NAO−) phases (e.g., Benedict et al. 2004; Luo et al. 2018; Minami and Takaya 2020; Ma and Liang 2023b; Zhao et al. 2023; Kim et al. 2024) and hence check their localized Lorenz energy cycle separately (refer to appendix B). After a careful check, we find that the main features are almost the same during NAO+ and NAO− and hence composite the energetics during NAO+ and NAO− together (refer to appendix B for details). Besides, the dynamics are found to be different for NAO in different seasons (e.g., Martineau et al. 2020); as a result, we focus only on NAO processes in the winter season; here, the winter season refers to November–March, including 5 months.

a. *Classical Lorenz energy cycle reproduced in a bulk view*

We first examine the canonical energy transfer in a bulk or integrated fashion between the low-frequency and high-frequency scales (Fig. 1). APE on the low-frequency window is found to be transferred to the high-frequency window during NAO (Fig. 1a). In contrast, KE experiences an inverse cascade; i.e., it is transferred from the high-frequency window to the low-frequency window (Fig. 1b). This reproduces a known fact on energy cascade in midlatitudes that the low-frequency window loses APE but gains KE, while the high-frequency window gains APE but loses KE. It is found that the buoyancy conversion from KE to APE dominates the low-frequency window (Fig. 1c), while that from APE to KE dominates the high-frequency window (Fig. 1d). In a bulk view, we can hence conclude that a net KE-to-APE conversion occurs on the low-frequency window, while a net APE-to-KE conversion dominates the high-frequency window. It is clear that these four processes form a loop path of the Lorenz energy cycle. Obviously, a loop path means that this energy cycle tends to sustain. This fact supports the previous findings that the low-frequency and high-frequency processes tend to form a positive feedback during NAO (e.g., Robinson 2000; Barnes and Hartmann 2010).

b. *Localized energetic processes*

Though in a bulk view the energetic processes are in agreement with the classical paradigm, by our computation, these four processes occur over different locations (Fig. 1). To be

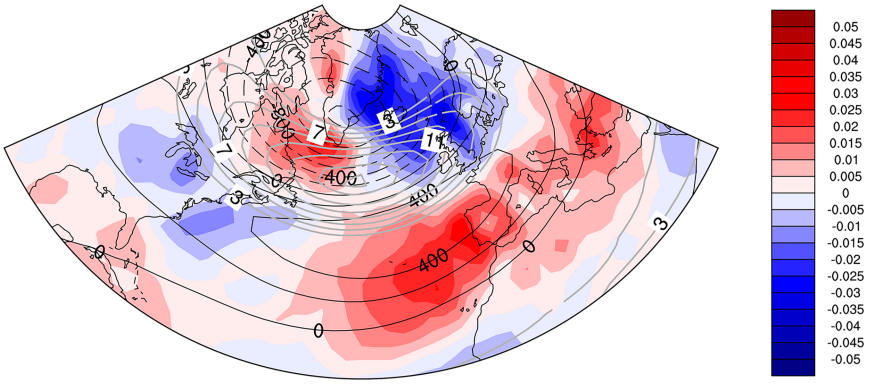

FIG. 4. Vertical velocity anomalies (shaded; $Pa\ s^{-1}$) projected onto the NAO index averaged from 500 hPa through 200 hPa. The black and gray contours represent the reconstructed geopotential ($m^2\ s^{-2}$) and zonal wind anomalies ($m\ s^{-1}$) on the low-frequency window projected onto the NAO index averaged from 500 hPa through 200 hPa. All the projections are fulfilled with Eq. (3).

specific, the canonical APE transfer from the low-frequency window to the high-frequency window is at the upstream of NAO (over the Labrador Sea; cf. Fig. 1a), while the KE transfer from the high-frequency window to the low-frequency window is at the downstream of NAO (over the ocean southwest of the British Isles; cf. Fig. 1b). The buoyancy conversion from KE to APE on the low-frequency window concentrates over the region southeast of Greenland (Fig. 1c). This observation implies that there must be some other processes which bridge these localized processes and hinge them together into a loop. A localized analysis is hence needed; it makes the focus of this study which we henceforth conduct.

1) ENERGETICS ON THE HIGH-FREQUENCY WINDOW

From the preceding section, we know that the high-frequency window gains APE upstream while losing KE downstream. In general, it gains mechanical energy upstream but loses mechanical energy downstream. A spatial redistribution of energy from upstream to downstream is thus anticipated by an energy conservation argument. Processes that can redistribute APE and KE on the high-frequency window are investigated here. For APE, transport is the only process. From Fig. 2a, indeed the APE transport process takes APE from upstream to downstream. For KE, there are two kinds of processes that can redistribute KE in space—KE transport and pressure work. We hence add them up. Figure 2b shows that these two processes together also transport KE from upstream to downstream.

So both the APE and KE on the high frequency are transported from upstream to downstream. These processes provide two paths of compensating the downstream KE loss through upscale feedback by the upstream APE gain through baroclinic instability. Path 1: APE is transported from upstream to downstream (Fig. 2a) and then converted to KE there (Fig. 1d). Path 2: APE is converted to KE upstream and then redistributed by KE transport and pressure work processes (Figs. 1d and 2b). These two paths connect the cross-scale APE processes upstream and the KE processes downstream.

2) ENERGETICS ON THE LOW-FREQUENCY WINDOW

Just like that on the high-frequency window, the gain of KE and loss of APE on the low-frequency window also occur at different sites (Figs. 1a,b). Following the procedure above, the KE transport and pressure work are added up (Fig. 3a). They behave to take KE from the region over the ocean southwest of the British Isles to the region southeast of Greenland. Recalling Fig. 1c, it is clear that southeast of Greenland is exactly where the KE is converted to APE. The APE transport process then carries APE from southeast of Greenland to the Labrador Sea (Fig. 3b). That is to say, there are three hotspots which are critical in the redistribution of energy on the low-frequency window, i.e., the region southwest of the British Isles, the region southeast of Greenland, and the Labrador Sea. By examining Figs. 1a and 1b, we can easily find that those over the southwest of the British Isles and over the Labrador Sea are exactly where the KE upscale feedback and baroclinic instability occur. Recalling the role of the hotspot southeast of Greenland, it acts like a "converter" which binds the other two hotspots together. It takes KE from the region southwest of the British Isles, converts it to APE, and then transports the converted APE to the region over the Labrador Sea. As a result, this converter links the upscale feedback and baroclinic instability together, by collecting KE from where the low-frequency window gains KE via upscale feedback and compensating APE loss from the low-frequency window where baroclinic instability occurs.

4. Dynamical implications of the localized Lorenz energy cycle

a. Vertical secondary circulations underlying NAO

In idealized models, a positive feedback is believed to be essential to NAO dynamics (e.g., Robinson 2000; Lorenz and Hartmann 2001; Barnes and Hartmann 2010). In this positive feedback, a secondary circulation is proposed to be important in the nonlinear dynamics of NAO (Robinson 2000). This secondary circulation is also inferred by Barnes and Hartmann (2010), based on the fact that upper divergence is aloft over the lower convergence, to close the NAO and eddy positive feedback loops. It hence deserves to investigate the real secondary circulations of the low-frequency NAO flow, which is done here through compositing analysis, from the observed (reanalysis) datasets. The composite vertical velocity field of the low-frequency NAO flow is shown in Fig. 4.

A direct observation is that the vertical motions are zonally in homogeneous. Actually, they reverse in the upstream and downstream of the NAO—the air sinks at the north and rises at the south in the upstream, while rising at the north and sinking at the south in the downstream. This makes sense since NAO is accompanied by a positive jet stream anomaly (shown by the gray contours in Fig. 4), and a jet stream leads to ascent (descent) motion at the south and descent (ascent) motion at the north in its entrance (exit) region (e.g., Keyser and Shapiro 1986; Uccellini and Kocin 1987). These facts show that the positive jet stream anomaly of NAO leads to two secondary circulations—one at its upstream and the other at its downstream—and they have reverse directions. Robinson (2000) and Barnes and Hartmann (2010) both show a signal of secondary circulation in their studies. However, the results here clearly show that there are two opposite secondary circulations. In this sense, a zonally uniform secondary circulation is not enough to tell the whole story of the positive feedback underlying NAO. We will show soon below that both these two secondary circulations are essential to NAO dynamics.

b. Reexamination of the positive feedback from an energetics viewpoint

In the positive feedback proposed by Robinson (2000), the low-frequency zonally mean vertical velocity anomalies tend to enhance the baroclinic eddy generation, which in turn strengthens the flow through more vigorous eddy momentum convergence. Clearly, the abovementioned positive feedback is accompanied by two kinds of energetic processes, i.e., the baroclinic instability and upscale KE transfer, since enhanced baroclinic eddy generation is essentially more vigorous baroclinic

instability, and enhanced eddy momentum convergence means positive KE transfer from the eddies to the flow. Castanheira and Marques (2019) verify these two positive processes in a zonal-mean energetics diagnostic study. However, the findings in our study tell us that the secondary circulations of NAO are zonally inhomogeneous and there are actually two opposite circulations upstream and downstream, respectively. The dynamics in a zonal-mean framework are not the whole story. A reexamination of energetics underlying the positive feedback with two secondary circulations is hence required. As shown above, the two secondary circulations are located at the entrance and exit regions of the jet stream anomaly of NAO, respectively. Accordingly, we will refer them to the entrance and exit secondary circulations.

Note that the cores of the northern branches of these two secondary circulations are located at the Labrador Sea and southeast of Greenland, respectively. We can quickly find that they share the same places with two of the hotspots in the localized Lorenz energy cycle discussed above, i.e., the G and L hotspots. This coincidence tells us that the G and L hotspots of the localized Lorenz energy cycle are closely related to the northern branches of the two secondary circulations, respectively. Recall that the dominant energetics processes over the G and L hotspots are buoyancy conversion from KE to APE (cf. Fig. 1c) and baroclinic instability of the low-frequency flow (cf. Fig. 1a). That is to say, the northern branches of the entrance and exit secondary circulations are closely related to, respectively, the buoyancy conversion from KE to APE and the baroclinic instability of the low-frequency flow. In Robinson's idealized work, these two physical processes are also necessary to form the positive feedback between the low-frequency flow and eddy forcing. The findings above confirm his conclusion. However, the processes we find here are actually different from their idealized counterparts. In Robinson's work, the KE of the flow gained from the eddy momentum convergence is directly converted into APE to enhance the baroclinicity of the flow through adiabatic heating at the sinking branch of the secondary circulation. In other words, the conversion from KE to APE and baroclinicity enhancement are both fulfilled by only one secondary circulation. In contrast, our results demonstrate that the entrance and exit secondary circulations are both involved—the task by one secondary circulation in Robinson's work is actually fulfilled by two secondary circulations. The exit one converts KE to APE, and then, the entrance one favors baroclinic instability.

Clearly, the two secondary circulations cannot form a direct positive feedback loop due to the inconsistency of the places where they act. This fact calls for extra processes linking the two circulations together to close the positive feedback. As shown in the last section, the "extra processes" include two kinds of candidates—those on the synoptic and the low-frequency window. On the low-frequency window, our findings here demonstrate that the APE gain from KE conversion at the rising branch of the exit secondary circulation is transported to the sinking branch of the entrance secondary circulation, and the baroclinicity of the flow is hence enhanced there. On the synoptic window, the extra processes turn out to be APE and KE transports from the western half to the eastern half of NAO and pressure work processes (Fig. 2). In other words, eddy propagation from the west to the east is essential to form the positive feedback. Robinson (2000) emphasizes the critical role of meridional propagation of the eddies in the feedback. Our results show that the zonal propagation is also essential to the feedback. To conclude, the implications here are that the zonal APE and KE transport processes, which are ignored in the previous zonally mean studies, are needed to be added to the positive feedback.

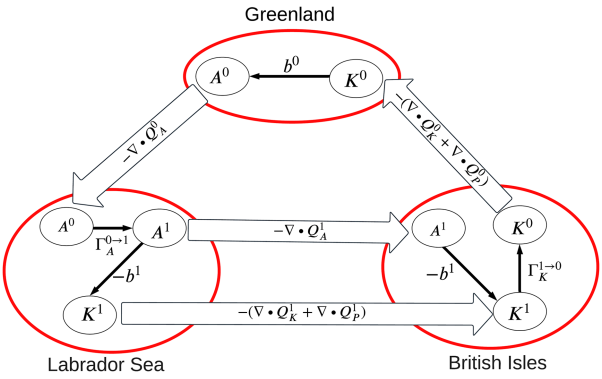

FIG. 5. A schematic diagram of the localized Lorenz energy cycle of NAO. The red circles represent the hotspots critical for the cycle. They are (top) that over the southeast of Greenland, (bottom left) that over the Labrador Sea, and (bottom right) that over the southwest of the British Isles. The A and K symbolize APE and KE, while the superscripts 1 and 0 represent the high-frequency window and the low-frequency window, respectively. The expressions $\nabla\cdot\mathbf{Q}_K$, $\nabla\cdot\mathbf{Q}_P$, Γ_A, Γ_K, and b signify KE transport, pressure work, canonical APE transfer, canonical KE transfer, and buoyancy conversion, respectively. The arrows indicate the paths of the energy cycle. For details of the localized energy cycle, please refer to Figs. 1–3.

5. Conclusions and discussion

To investigate the multiscale interaction underlying the NAO, a localized Lorenz energy cycle is constructed for the first time in this study by taking advantage of the localized nature of a functional analysis apparatus, namely, multiscale window transform (MWT), and the MWT-based methodology for localized multiscale energetics analysis. This generalizes the previous global formalisms, in which all the processes are spatially averaged, with local information lost.

Intriguing localized features have been found from the spatial distributions of energetics (cf. section 3); they can be summarized schematically in Fig. 5. As elaborated in section 3, there are three hotspots in the localized Lorenz energy cycle: one over the southeast of Greenland (the top), one over the Labrador Sea (bottom left), and one over the southwest of the British Isles (bottom right). In the diagram, they are denoted by the red circles and will be referred to as G, L, and B hotspots hereafter. Focusing on these circles, we can find that they are connected via transport and pressure work processes which only carry energy through physical space on the same scale window, i.e., the high-frequency or the low-frequency

window. Further examination of it tells us that the G hotspot connects with the others on the low-frequency window, while the other two hotspots connect themselves on the high-frequency window. These two windows are bridged by the processes over the L and B hotspots through APE and KE transfer processes, respectively. APE is transferred from the low-frequency window to the high-frequency window over the L hotspot, while KE is transferred back from the high-frequency window to the low-frequency window over the B hotspot. In this sense, the L and B hotspots are converters linking different scales. For the G hotspot, it works as a converter linking different forms of energy, i.e., KE and APE. In a word, the connections between scales and energy forms are built by the in situ processes over the hotspots, and the hotspots are linked via transport and pressure work processes.

The dynamical implications of the resulting energy cycle are also discussed. Two secondary circulations are found accompanying the jet stream anomaly of NAO—one at its entrance region and the other at the exit region. We hence call them entrance and exit secondary circulations, respectively. The G and L hotspots are actually where the northern branches of the exit and entrance secondary circulations exist. At the G hotspot, KE is converted to APE. The gained APE is then transported to the L hotspot. These facts demonstrate that these two processes fulfilled by only one secondary circulation in idealized models (e.g., Robinson 2000) are actually completed by two secondary circulations at the entrance and exit of the NAO jet stream. Besides, the upscale forcing from the synoptic eddies to the low-frequency flow occurs neither at the entrance secondary circulation nor at the exit one but at the B hotspot. Clearly, the three essential processes in the classical positive feedback—conversion from KE to APE, baroclinicity enhancement, and synoptic eddies upscale forcing—occur in different regions. They are connected by the energy transport and pressure work process to form a localized energy loop, as shown in Fig. 5. Note that Robinson (2000) has emphasized the importance of the meridional transport of the eddies; here, we show that the zonal transport is also important. The implication of this study is that the two secondary circulations, i.e., the entrance and the exit secondary circulations of the NAO jet stream, plus their respective zonal variations, are needed when the mechanism underlying the positive feedback is discussed.

The results may also be interpreted from the perspective of low-frequency modulation of NAO on the mean flow and transient eddy interactions (thanks are due to an anonymous reviewer for pointing out this). Recall that the interactions between the mean flow and transient eddies are most representative at the storm tracks, involving a strong jet stream and abundant synoptic eddies, and the main characteristics of the interactions there are as below: Strong eddy-induced westerly momentum convergence only occurs at the downstream of the jet stream, but the upstream (e.g., Blackmon et al. 1977); from the perspective of multiscale energetics, the mean flow fuels synoptic eddies at the entrance of the storm track via baroclinic instability; the eddies then propagate downstream and feed KE back to the mean flow at the exit of the storm track (e.g., Chang et al. 2002). Our results here also show the above characteristics. This means that the modulations of NAO on the interactions between the mean flow and eddies do not change their basic patterns but only enhance their strengths. It is understandable considering that the NAO is accompanied by a strengthened jet and storm track, and more vigorous interactions are hence naturally anticipated. In this sense, the baroclinic instability in the upstream of the NAO, the propagation of KE and APE of the eddies from the upstream to the downstream, and the inverse barotropic KE transfer from the eddies to the basic flow found in this study are physically consistent with the well-known interactions between the jet stream and eddies in the storm-track regions (e.g., Simmons and Hoskins 1978; Hoskins et al. 1983; Holopainen 1984; Lee and Mak 1996; Chang et al. 2002) and also consistent with the corresponding physical interpretations (e.g., Lau and Holopainen 1984; Hoskins and Valdes 1990; Lau and Nath 1991; Chang 1993; Lee 1995; Swanson et al. 1997; Chang et al. 2002) in previous studies. To be specific, the baroclinicity of the flow in the jet entrance regions, which fuels the eddies, is found to be partially maintained by latent heating (Hoskins and Valdes 1990) and surface drag (Robinson 1996, 2000). For the eddy energy transport from the upstream to the downstream, it involves many kinds of physical processes, including wave propagation (e.g., Robinson 1996, 2000), the advection by the flow (Lee and Mak 1996), and nonlinear wave packet downstream development (Orlanski and Katzfey 1991; Chang 1993; Chang and Orlanski 1993, 1994); the downstream development here refers to the eddies in a wave packet transporting energy to their downstream counterparts (see Chang et al. 2002). At the jet exit, the eddy anisotropy tends to be enhanced and hence the eddies lose energy to the mean flow irreversibly where the zonal winds are relatively weak, explaining the preferred upscale KE transfer from the eddies to the mean flow in the presence of relatively weak zonal winds there (Hoskins et al. 1983; Lee 1995; Swanson et al. 1997).

Besides the basic processes of the interactions described above, an essential issue underlying the modulation of low-frequency variabilities on the interactions of basic flow and eddies is a positive feedback between the low-frequency variabilities and the eddies (e.g., Cai and Mak 1990; Robinson 1991; Branstator 1995; Feldstein 2003; Luo 2005; Luo et al. 2019). Our findings here illustrate how this feedback is closed from a perspective of multiscale energetics. Besides the above basic interactive processes between the low-frequency flow and eddies, the buoyancy conversion and APE transport on the low-frequency scale are also found essential to close the positive feedback, which respectively convert the KE gained from the eddy upscale KE transfer to APE and then transport APE to where the eddies grow through baroclinic instability, connecting all the nodes in the feedback loop. In this loop, the results here show that the energy of low-frequency processes tends to be transported westward, consistent with the results of Hoskins et al. (1983).

This study is conducted in the context of two-scale window decomposition. Whenever needed, a three-scale window decomposition can be easily implemented in the MWT-based framework, where the asymmetric dynamics of the low-frequency NAO+ and NAO− events and the effects of the background

on that can be investigated (e.g., Ma and Liang 2023b). Besides, the NAO undergoes interannual and decadal variabilities under global warming (e.g., Ulbrich and Christoph 1999; Jung et al. 2003; Luo et al. 2010; Dong et al. 2011; Yang et al. 2024); how the localized Lorenz energy cycle found in this study may change hence makes another important topic. This, among other issues, will be explored in future studies.

Acknowledgments. We are grateful to three anonymous referees whose constructive advice helped improve the manuscript. This study was partially supported by the National Natural Science Foundation of China (42230105, 42005052, 41975064), by the Southern Marine Science and Engineering Guangdong Laboratory (Zhuhai) (SML2023SP203, 313022003, 313022005), by Fudan University through the Startup Foundation (IDH2318009Y), by the Shanghai B and R Joint Laboratory Project (22230750300), and by the Shanghai International Science and Technology Partnership Project (21230780200).

Data availability statement. The ERA-40 and ERA5 datasets in this study are from https://apps-dev.ecmwf.int/datasets/data/era40-daily/levtype=pl/ and https://cds.climate.copernicus.eu/datasets/reanalysis-era5-pressure-levels?tab=download, respectively. The NAO index is obtained from https://ftp.cpc.ncep.noaa.gov/cwlinks/norm.daily.nao.cdas.z500.19500101_current.csv.

APPENDIX A

Localized Lorenz Energy Cycle during NAO in the Lower Troposphere

The interactions between the flow and eddies are found to be different in the upper and lower troposphere. For example, Lau and Nath (1991) found that the eddy-induced vorticity forcing and the heat forcing to the flow are out of phase in the upper troposphere but in phase in the lower troposphere. Here, we found that the localized Lorenz energy cycles are also different in the upper (Figs. 1–3) and lower troposphere (Figs. A1–A3). The main point here is that the closed Lorenz energy cycle in the upper troposphere does not hold in the lower troposphere, lacking one critical process—the KE transfer from the eddies to the flow (see Fig. A1b). This finding is consistent with Hoskins et al. (1983), who found that the eddies tend to propagate upward and then lose their energy to enforce the flow in the upper troposphere. Besides, the energy transport of eddies from the upstream to the downstream is also insignificant as compared to their counterparts in the upper troposphere.

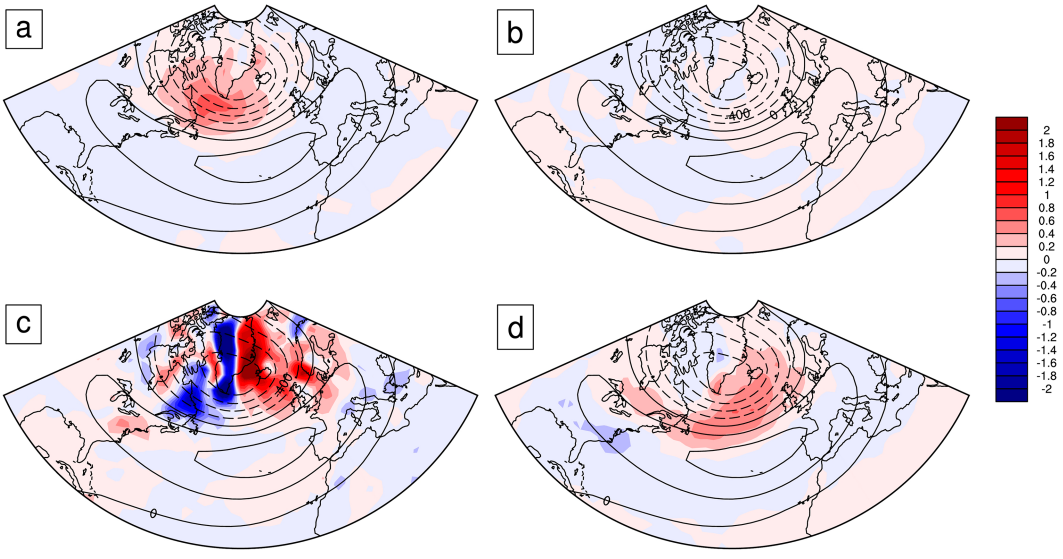

FIG. A1. The fields of baroclinic/barotropic transfers and buoyancy conversion superimposed with geopotential. The contoured are geopotential anomalies from the climatology projected onto the NAO index at 500 hPa ($m^2\ s^{-2}$). The shaded are (a) APE transfer from the low-frequency window to the high-frequency window ($\Gamma_A^{0\to1}$; $10^{-3}\ m^2\ s^{-3}$), (b) KE transfer from the high-frequency window to the low-frequency window ($\Gamma_K^{1\to0}$; $10^{-3}\ m^2\ s^{-3}$), (c) buoyancy conversion from KE to APE on the low-frequency window (b^0; $10^{-3}\ m^2\ s^{-3}$), and (d) buoyancy conversion from APE to KE on the high-frequency window ($-b^1$; $10^{-3}\ m^2\ s^{-3}$) anomalies from their respective climatologies projected onto the NAO index averaged from 1000 hPa through 500 hPa. All the projections are fulfilled with Eq. (3).

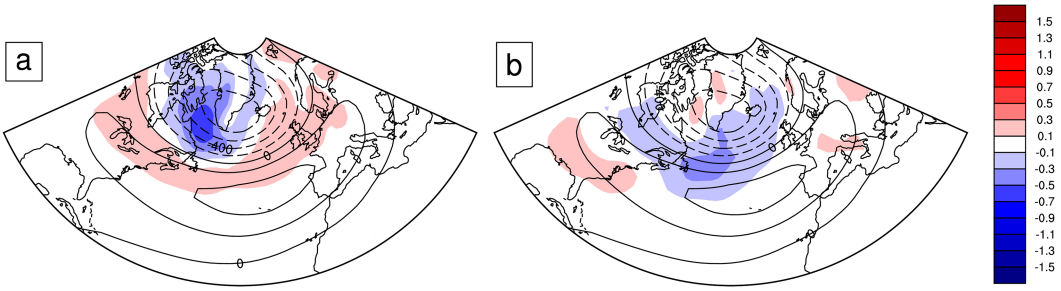

FIG. A2. High-frequency energy spatial redistribution. The contoured are geopotential anomalies from the climatology projected onto the NAO index at 500 hPa ($m^2\ s^{-2}$). The shaded are (a) APE transport on the high-frequency window ($-\nabla\cdot\mathbf{Q}_A^1$; $10^{-3}\ m^2\ s^{-3}$) and (b) KE transport and pressure work on the high-frequency window ($-\nabla\cdot\mathbf{Q}_K^1 - \nabla\cdot\mathbf{Q}_P^1$; $10^{-3}\ m^2\ s^{-3}$) anomalies to their climatologies projected onto the NAO index averaged from 1000 hPa through 500 hPa. All the projections are fulfilled with Eq. (3).

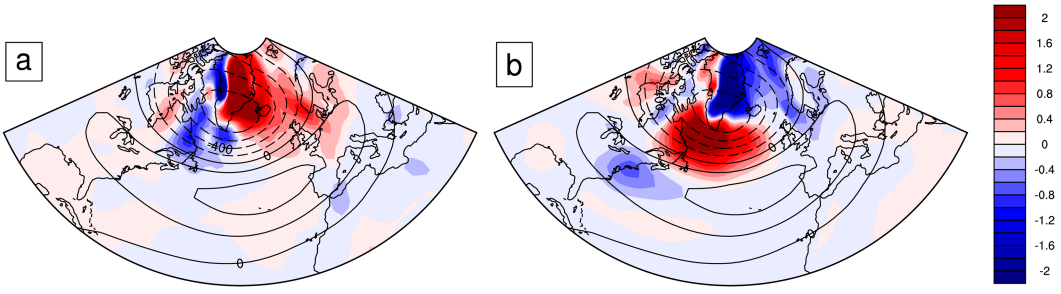

FIG. A3. Low-frequency energy spatial redistribution. Superimposed are the geopotential anomalies to their climatology projected onto the NAO index at 500 hPa (contoured; $m^2\ s^{-2}$). The shaded are (a) KE transport and pressure work on the low-frequency window ($-\nabla\cdot\mathbf{Q}_K^0 - \nabla\cdot\mathbf{Q}_K^0$; $10^{-3}\ m^2\ s^{-3}$) and (b) APE transport on the low-frequency window ($-\nabla\cdot\mathbf{Q}_A^0$; $10^{-3}\ m^2\ s^{-3}$) anomalies from their respective climatologies projected onto the NAO index averaged from 1000 hPa through 500 hPa. All the projections are fulfilled with Eq. (3).

APPENDIX B

Localized Lorenz Energy Cycles Projected to NAO+ and NAO−

The dynamics underlying the NAO-positive (NAO+) and NAO-negative (NAO−) phases are found to be asymmetric (e.g., Benedict et al. 2004; Luo et al. 2018; Minami and Takaya 2020; Ma and Liang 2023b; Zhao et al. 2023; Kim et al. 2024). We hence investigate the localized Lorenz energy cycles during NAO+ and NAO− separately. The projected energetics and geopotential anomalies during NAO+ and NAO− are displayed in Figs. B1–B3 and B4–B6, respectively. The projection procedure is fulfilled according to the same procedure as described in section 3. Note that, in performing the projection for a variable, say, VAR, it is multiplied by the NAO index I, so during NAO−, the sign is reversed, since the NAO index I is negative. As a result, the anomalies of energetics and geopotential share the same sign in Figs. B1–B3 and B4–B6. Checking on the main features of the energetics during NAO+ and NAO−, the asymmetry between NAO+ and NAO− is confirmed here—the magnitudes of the energetics are stronger in Figs. B4–B6 than those in Figs. B1–B3, reflecting the strength asymmetry of NAO+ and NAO−, consistent with the previous studies (e.g., Benedict et al. 2004; Luo et al. 2018; Minami and Takaya 2020; Ma and Liang 2023b; Zhao et al. 2023; Kim et al. 2024). However, as clearly seen, this asymmetry does not affect the main findings in this study—the localized Lorenz energy cycle is supported in both NAO+ and NAO−. It is hence justifiable to composite the projected results in these two phases together, as we do in the main text.

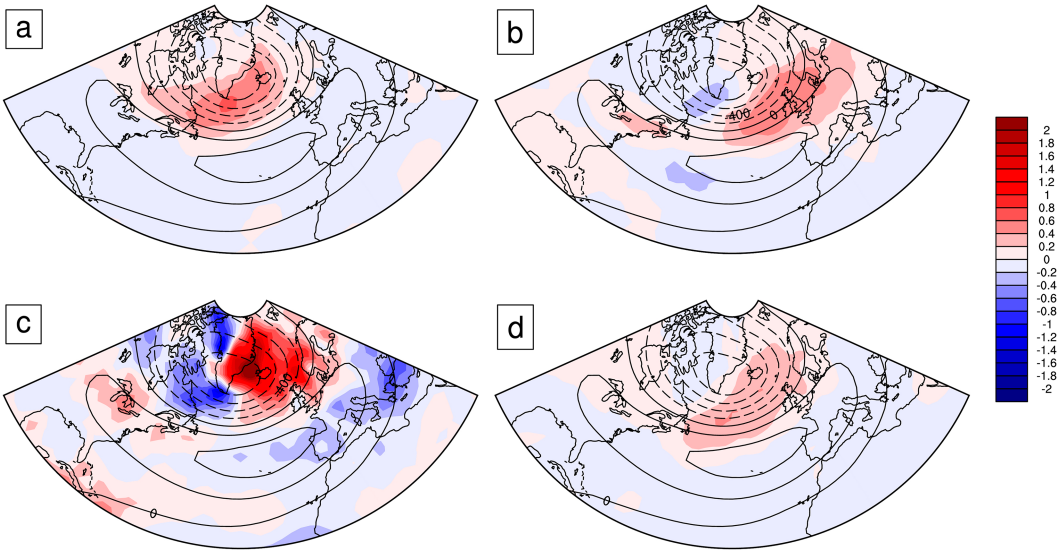

FIG. B1. The fields of baroclinic/barotropic transfers and buoyancy conversion superimposed with geopotential. The contoured are geopotential anomalies from the climatology projected onto the NAO+ index at 500 hPa ($m^2\ s^{-2}$). The shaded are (a) APE transfer from the low-frequency window to the high-frequency window ($\Gamma_A^{0\to1}$; $10^{-3}\ m^2\ s^{-3}$), (b) KE transfer from the high-frequency window to the low-frequency window ($\Gamma_K^{1\to0}$; $10^{-3}\ m^2\ s^{-3}$), (c) buoyancy conversion from KE to APE on the low-frequency window (b^0; $10^{-3}\ m^2\ s^{-3}$), and (d) buoyancy conversion from APE to KE on the high-frequency window ($-b^1$; $10^{-3}\ m^2\ s^{-3}$) anomalies from their respective climatologies projected onto the NAO+ index averaged from 500 hPa through 200 hPa. All the projections are fulfilled with Eq. (3).

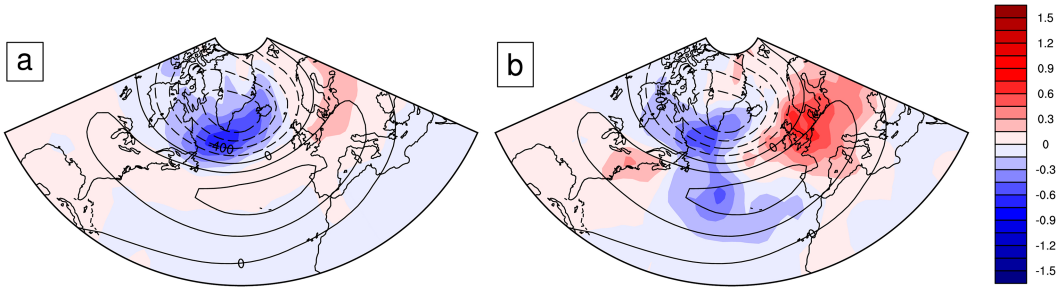

FIG. B2. High-frequency energy spatial redistribution. The contoured are geopotential anomalies from the climatology projected onto the NAO+ index at 500 hPa ($m^2\ s^{-2}$). The shaded are (a) APE transport on the high-frequency window ($-\nabla\cdot\mathbf{Q}_A^1$; $10^{-3}\ m^2\ s^{-3}$) and (b) KE transport and pressure work on the high-frequency window ($-\nabla\cdot\mathbf{Q}_K^1 - \nabla\cdot\mathbf{Q}_P^1$; $10^{-3}\ m^2\ s^{-3}$) anomalies to their climatology projected onto the NAO+ index averaged from 500 hPa through 200 hPa. All the projections are fulfilled with Eq. (3).

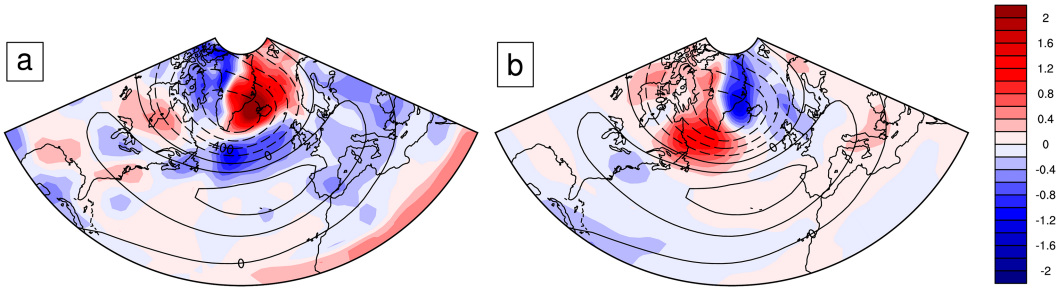

FIG. B3. Low-frequency energy spatial redistribution. Superimposed are the geopotential anomalies to their climatology projected onto the NAO+ index at 500 hPa (contoured; $m^2\ s^{-2}$). The shaded are (a) KE transport and pressure work on the low-frequency window ($-\nabla\cdot\mathbf{Q}_K^0 - \nabla\cdot\mathbf{Q}_K^0$; $10^{-3}\ m^2\ s^{-3}$) and (b) APE transport on the low-frequency window ($-\nabla\cdot\mathbf{Q}_A^0$; $10^{-3}\ m^2\ s^{-3}$) anomalies from their respective climatologies projected onto the NAO+ index averaged from 500 hPa through 200 hPa. All the projections are fulfilled with Eq. (3).

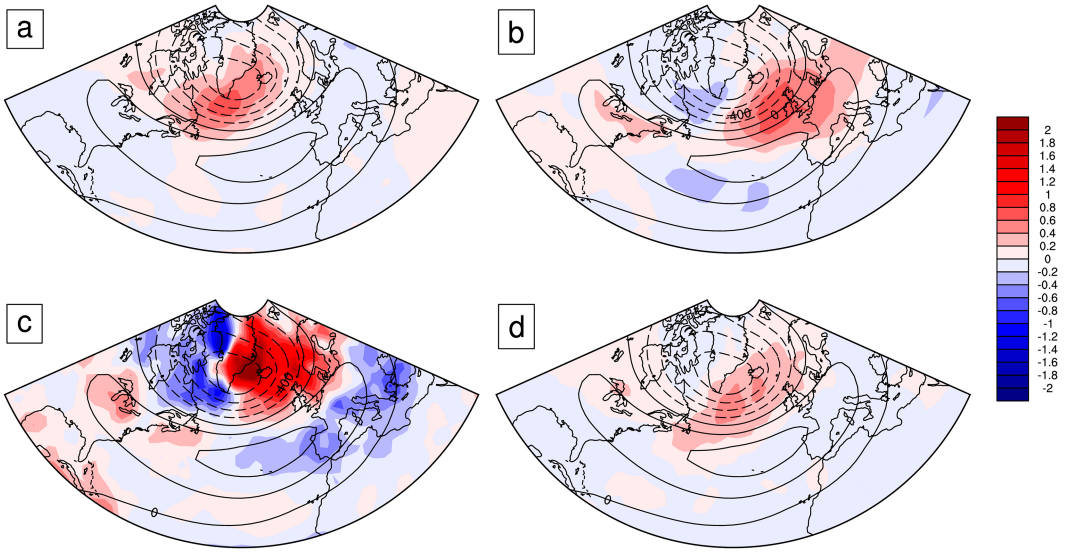

FIG. B4. As in Fig. B1, but that the energetics and geopotential are for NAO−.

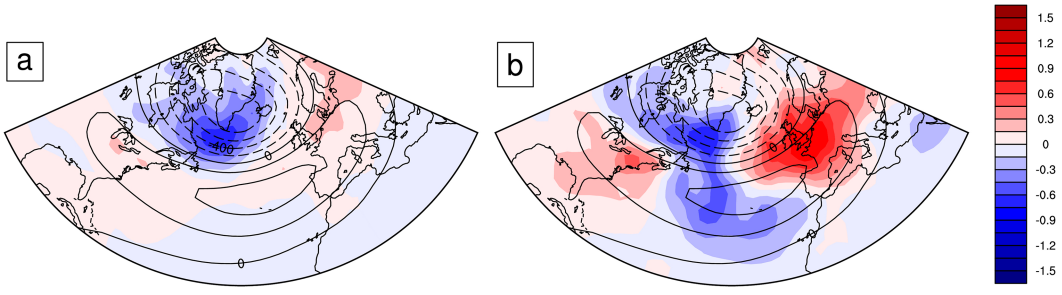

FIG. B5. As in Fig. B2, but that the energetics and geopotential are for NAO−.

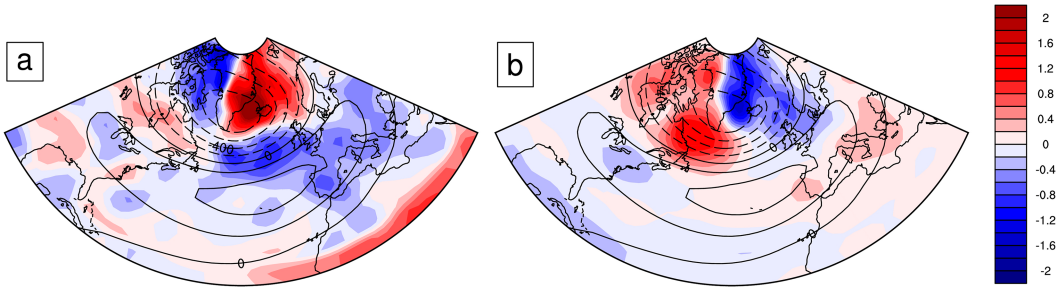

FIG. B6. As in Fig. B3, but that the energetics and geopotential are for NAO−.

REFERENCES

Barnes, E. A., and D. L. Hartmann, 2010: Dynamical feedbacks and the persistence of the NAO. *J. Atmos. Sci.*, **67**, 851–865, https://doi.org/10.1175/2009JAS3193.1.

——, ——, D. M. W. Frierson, and J. Kidston, 2010: Effect of latitude on the persistence of eddy-driven jets. *Geophys. Res. Lett.*, **37**, L11804, https://doi.org/10.1029/2010GL043199.

——, S. M. Samarasinghe, I. Ebert-Uphoff, and J. C. Furtado, 2019: Tropospheric and stratospheric causal pathways between the MJO and NAO. *J. Geophys. Res. Atmos.*, **124**, 9356–9371, https://doi.org/10.1029/2019JD031024.

Barnston, A. G., and R. E. Livezey, 1987: Classification, seasonality and persistence of low-frequency atmospheric circulation patterns. *Mon. Wea. Rev.*, **115**, 1083–1126, https://doi.org/10.1175/1520-0493(1987)115<1083:CSAPOL>2.0.CO;2.

Benedict, J. J., S. Lee, and S. B. Feldstein, 2004: Synoptic view of the North Atlantic Oscillation. *J. Atmos. Sci.*, **61**, 121–144, https://doi.org/10.1175/1520-0469(2004)061<0121:SVOTNA>2.0.CO;2.

Blackmon, M. L., J. M. Wallace, N.-C. Lau, and S. L. Mullen, 1977: An observational study of the Northern Hemisphere wintertime circulation. *J. Atmos. Sci.*, **34**, 1040–1053, https://doi.org/10.1175/1520-0469(1977)034%3C1040:AOSOTN%3E2.0.CO;2.

Branstator, G., 1995: Organization of storm track anomalies by recurring low-frequency circulation anomalies. *J. Atmos. Sci.*, **52**, 207–226, https://doi.org/10.1175/1520-0469(1995)052<0207:OOSTAB>2.0.CO;2.

Cai, M., and M. Mak, 1990: Symbiotic relation between planetary and synoptic-scale waves. *J. Atmos. Sci.*, **47**, 2953–2968, https://doi.org/10.1175/1520-0469(1990)047<2953:SRBPAS>2.0.CO;2.

Castanheira, J. M., and C. A. F. Marques, 2019: The energy cascade associated with daily variability of the North Atlantic Oscillation. *Quart. J. Roy. Meteor. Soc.*, **145**, 197–210, https://doi.org/10.1002/qj.3422.

Chang, E. K. M., 1993: Downstream development of baroclinic waves as inferred from regression analysis. *J. Atmos. Sci.*, **50**, 2038–2053, https://doi.org/10.1175/1520-0469(1993)050<2038:DDOBWA>2.0.CO;2.

——, and I. Orlanski, 1993: On the dynamics of a storm track. *J. Atmos. Sci.*, **50**, 999–1015, https://doi.org/10.1175/1520-0469(1993)050<0999:OTDOAS>2.0.CO;2.

——, and ——, 1994: On energy flux and group velocity of waves in baroclinic flows. *J. Atmos. Sci.*, **51**, 3823–3828, https://doi.org/10.1175/1520-0469(1994)051<3823:OEFAGV>2.0.CO;2.

——, S. Lee, and K. L. Swanson, 2002: Storm track dynamics. *J. Climate*, **15**, 2163–2183, https://doi.org/10.1175/1520-0442(2002)015<02163:STD>2.0.CO;2.

Cohen, J., and M. Barlow, 2005: The NAO, the AO, and global warming: How closely related? *J. Climate*, **18**, 4498–4513, https://doi.org/10.1175/JCLI3530.1.

Dong, B., R. T. Sutton, and T. Woollings, 2011: Changes of interannual NAO variability in response to greenhouse gases forcing. *Climate Dyn.*, **37**, 1621–1641, https://doi.org/10.1007/s00382-010-0936-6.

Feldstein, S., 2003: The dynamics of NAO teleconnection pattern growth and decay. *Quart. J. Roy. Meteor. Soc.*, **129**, 901–924, https://doi.org/10.1256/qj.02.76.

——, and S. Lee, 1998: Is the atmospheric zonal index driven by an eddy feedback? *J. Atmos. Sci.*, **55**, 3077–3086, https://doi.org/10.1175/1520-0469(1998)055<3077:ITAZID>2.0.CO;2.

Guo, Z., and X. San Liang, 2022: Nexus of ambient flow and squall line via turbulence in the March 2018 meso-scale convective system over Southeast China. *Atmos. Res.*, **277**, 106287, https://doi.org/10.1016/j.atmosres.2022.106287.

Hansen, A. R., and A. Sutera, 1984: A comparison of the spectral energy and enstrophy budgets of blocking versus nonblocking periods. *Tellus*, **36A**, 52–63, https://doi.org/10.1111/j.1600-0870.1984.tb00222.x.

Hersbach, H., and Coauthors, 2020: The ERA5 global reanalysis. *Quart. J. Roy. Meteor. Soc.*, **146**, 1999–2049, https://doi.org/10.1002/qj.3803.

Holopainen, E., 1984: Statistical local effect of synoptic-scale transient eddies on the time-mean flow in the northern extratropics in winter. *J. Atmos. Sci.*, **41**, 2505–2515, https://doi.org/10.1175/1520-0469(1984)041<2505:SLEOSS>2.0.CO;2.

Hoskins, B. J., and P. J. Valdes, 1990: On the existence of storm-tracks. *J. Atmos. Sci.*, **47**, 1854–1864, https://doi.org/10.1175/1520-0469(1990)047<1854:OTEOST>2.0.CO;2.

——, I. N. James, and G. H. White, 1983: The shape, propagation and mean-flow interaction of large-scale weather systems. *J. Atmos. Sci.*, **40**, 1595–1612, https://doi.org/10.1175/1520-0469(1983)040<1595:TSPAMF>2.0.CO;2.

Hurrell, J. W., 1995: Decadal trends in the North Atlantic Oscillation: Regional temperatures and precipitation. *Science*, **269**, 676–679, https://doi.org/10.1126/science.269.5224.676.

——, 1996: Influence of variations in extratropical wintertime teleconnections on Northern Hemisphere temperature. *Geophys. Res. Lett.*, **23**, 665–668, https://doi.org/10.1029/96GL00459.

——, and C. Deser, 2009: North Atlantic climate variability: The role of the North Atlantic Oscillation. *J. Mar. Syst.*, **78**, 28–41, https://doi.org/10.1016/j.jmarsys.2008.11.026.

Jin, F.-F., 2010: Eddy-induced instability for low-frequency variability. *J. Atmos. Sci.*, **67**, 1947–1964, https://doi.org/10.1175/2009JAS3185.1.

——, L.-L. Pan, and M. Watanabe, 2006a: Dynamics of synoptic eddy and low-frequency flow interaction. Part I: A linear closure. *J. Atmos. Sci.*, **63**, 1677–1694, https://doi.org/10.1175/JAS3715.1.

——, ——, and ——, 2006b: Dynamics of synoptic eddy and low-frequency flow interaction. Part II: A Theory for low-frequency modes. *J. Atmos. Sci.*, **63**, 1695–1708, https://doi.org/10.1175/JAS3716.1.

Jung, T., M. Hilmer, E. Ruprecht, S. Kleppek, S. K. Gulev, and O. Zolina, 2003: Characteristics of the recent eastward shift of interannual NAO variability. *J. Climate*, **16**, 3371–3382, https://doi.org/10.1175/1520-0442(2003)016%3C3371:COTRES%3E2.0.CO;2.

Kenyon, J., and G. C. Hegerl, 2008: Influence of modes of climate variability on global temperature extremes. *J. Climate*, **21**, 3872–3889, https://doi.org/10.1175/2008JCLI2125.1.

Keyser, D., and M. A. Shapiro, 1986: A review of the structure and dynamics of upper-level frontal zones. *Mon. Wea. Rev.*, **114**, 452–499, https://doi.org/10.1175/1520-0493(1986)114<0452:AROTSA>2.0.CO;2.

Kim, M., C. Yoo, M.-K. Sung, and S. Lee, 2021: Classification of wintertime atmospheric teleconnection patterns in the Northern Hemisphere, *J. Climate*, **34**, 1847–1861, https://doi.org/10.1175/JCLI-D-20-0339.1.

——, M.-K. Sung, and C. Yoo, 2024: Phase dependence of growth mechanisms in the daily energetics of the North Atlantic Oscillation. *Quart. J. Roy. Meteor. Soc.*, **150**, 1566–1580, https://doi.org/10.1002/qj.4659.

Kug, J.-S., and F.-F. Jin, 2009: Left-hand rule for synoptic eddy feedback on low-frequency flow. *Geophys. Res. Lett.*, **36**, L05709, https://doi.org/10.1029/2008GL036435.

Kushnir, Y., 1987: Retrograding wintertime low-frequency disturbances over the North Pacific Ocean. *J. Atmos. Sci.*, **44**, 2727–2742, https://doi.org/10.1175/1520-0469(1987)044<2727:RWLFDO>2.0.CO;2.

Lau, N.-C., and E. O. Holopainen, 1984: Transient eddy forcing of the time-mean flow as identified by geopotential tendencies. *J. Atmos. Sci.*, **41**, 313–328, https://doi.org/10.1175/1520-0469(1984)041<0313:TEFOTT>2.0.CO;2.

——, and M. J. Nath, 1991: Variability of the baroclinic and barotropic transient eddy forcing associated with monthly changes in the midlatitude storm tracks. *J. Atmos. Sci.*, **48**, 2589–2613, https://doi.org/10.1175/1520-0469(1991)048<2589:VOTBAB>2.0.CO;2.

Lee, S., 1995: Localized storm tracks in the absence of local instability. *J. Atmos. Sci.*, **52**, 977–989, https://doi.org/10.1175/1520-0469(1995)052<0977:LSTITA>2.0.CO;2.

Lee, W.-J., and M. Mak, 1996: The role of orography in the dynamics of storm tracks. *J. Atmos. Sci.*, **53**, 1737–1750, https://doi.org/10.1175/1520-0469(1996)053%3C1737:TROOIT%3E2.0.CO;2.

Limpasuvan, V., and D. L. Hartmann, 1999: Eddies and the annular modes of climate variability. *Geophys. Res. Lett.*, **26**, 3133–3136, https://doi.org/10.1029/1999GL010478.

Liang, X. San, 2016: Canonical transfer and multiscale energetics for primitive and quasigeostrophic atmospheres. *J. Atmos. Sci.*, **73**, 4439–4468, https://doi.org/10.1175/JAS-D-16-0131.1.

——, and A. R. Robinson, 2005: Localized multiscale energy and vorticity analysis: I. Fundamentals. *Dyn. Atmos. Oceans*, **38**, 195–230, https://doi.org/10.1016/j.dynatmoce.2004.12.004.

——, and ——, 2007: Localized multi-scale energy and vorticity analysis II. Finite-amplitude instability theory and validation. *Dyn. Atmos. Oceans*, **44**, 51–76, https://doi.org/10.1016/j.dynatmoce.2007.04.001.

——, and D. G. M. Anderson, 2007: Multiscale window transform. *Multiscale Model. Simul.*, **6**, 437–467, https://doi.org/10.1137/06066895X.

Lorenz, D. J., and D. L. Hartmann, 2001: Eddy–zonal flow feedback in the Southern Hemisphere. *J. Atmos. Sci.*, **58**, 3312–3327, https://doi.org/10.1175/1520-0469(2001)058<3312:EZFFIT>2.0.CO;2.

——, and ——, 2003: Eddy–zonal flow feedback in the Northern Hemisphere Winter. *J. Climate*, **16**, 1212–1227, https://doi.org/10.1175/1520-0442(2003)16<1212:EFFITN>2.0.CO;2.

Lorenz, E. N., 1955: Available potential energy and the maintenance of the general circulation. *Tellus*, **7A** (2), 157–167, https://doi.org/10.1111/j.2153-3490.1955.tb01148.x.

Luo, D., 2005: A barotropic envelope Rossby soliton model for block–eddy interaction. Part I: Effect of topography. *J. Atmos. Sci.*, **62**, 5–21, https://doi.org/10.1175/1186.1.

——, A. R. Lupo, and H. Wan, 2007a: Dynamics of eddy-driven low-frequency dipole modes. Part I: A simple model of North Atlantic Oscillations. *J. Atmos. Sci.*, **64**, 3–28, https://doi.org/10.1175/JAS3818.1.

——, T. Gong, and Y. Diao, 2007b: Dynamics of eddy-driven low-frequency dipole modes. Part III: Meridional displacement of westerly jet anomalies during two phases of NAO. *J. Atmos. Sci.*, **64**, 3232–3248, https://doi.org/10.1175/JAS3998.1.

——, Z. Zhu, R. Ren, L. Zhong, and C. Wang, 2010: Spatial pattern and zonal shift of the North Atlantic Oscillation. Part I: A dynamical interpretation. *J. Atmos. Sci.*, **67**, 2805–2826, https://doi.org/10.1175/2010JAS3345.1.

——, L. Zhong, and C. L. E. Franzke, 2015: Inverse energy cascades in an eddy-induced NAO-type flow: Scale interaction mechanism. *J. Atmos. Sci.*, **72**, 3417–3448, https://doi.org/10.1175/JAS-D-15-0062.1.

——, X. Chen, and S. B. Feldstein, 2018: Linear and nonlinear dynamics of North Atlantic Oscillations: A new thinking of symmetry breaking. *J. Atmos. Sci.*, **75**, 1955–1977, https://doi.org/10.1175/JAS-D-17-0274.1.

——, W. Zhang, L. Zhong, and A. Dai, 2019: A nonlinear theory of atmospheric blocking: A potential vorticity gradient view. *J. Atmos. Sci.*, **76**, 2399–2427, https://doi.org/10.1175/JAS-D-18-0324.1.

Ma, J., and X. San Liang, 2017: Multiscale dynamical processes underlying the wintertime Atlantic blockings. *J. Atmos. Sci.*, **74**, 3815–3831, https://doi.org/10.1175/JAS-D-16-0295.1.

——, and ——, 2023a: Upstream–downstream asymmetry in multiscale interaction underlying the Northern Hemisphere atmospheric blockings. *J. Atmos. Sci.*, **80**, 1995–2011, https://doi.org/10.1175/JAS-D-22-0220.1.

——, and ——, 2023b: Distinctly different dynamical processes in maintaining the intraseasonal NAO+ and NAO−. *Geophys. Res. Lett.*, **50**, e2023GL103351, https://doi.org/10.1029/2023GL103351.

——, ——, and D. Chen, 2023: The role of multiscale interaction in the maintenance and propagation of MJO in boreal winter. *J. Climate*, **36**, 7827–7846, https://doi.org/10.1175/JCLI-D-23-0332.1.

Martineau, P., H. Nakamura, Y. Kosaka, and A. Yamamoto, 2020: Importance of a vertically tilting structure for energizing the North Atlantic Oscillation. *Sci. Rep.*, **10**, 12671, https://doi.org/10.1038/s41598-020-69551-5.

Minami, A., and Y. Takaya, 2020: Enhanced Northern Hemisphere correlation skill of subseasonal predictions in the strong negative phase of the Arctic Oscillation. *J. Geophys. Res. Atmos.*, **125**, e2019JD031268, https://doi.org/10.1029/2019JD031268.

Orlanski, I., and J. Katzfey, 1991: The life cycle of a cyclone wave in the Southern Hemisphere. Part I: Eddy energy budget. *J. Atmos. Sci.*, **48**, 1972–1998, https://doi.org/10.1175/1520-0469(1991)048<1972:TLCOAC>2.0.CO;2.

Plumb, R. A., 1983: A new look at the energy cycle. *J. Atmos. Sci.*, **40**, 1669–1688, https://doi.org/10.1175/1520-0469(1983)040<1669:ANLATE>2.0.CO;2.

Ren, H.-L., F.-F. Jin, J.-S. Kug, J.-X. Zhao, and J. Park, 2009: A kinematic mechanism for positive feedback between synoptic eddies and NAO. *Geophys. Res. Lett.*, **36**, L11709, https://doi.org/10.1029/2009GL037294.

——, ——, and L. Gao, 2012: Anatomy of synoptic eddy–NAO interaction through eddy structure decomposition. *J. Atmos. Sci.*, **69**, 2171–2191, https://doi.org/10.1175/JAS-D-11-069.1.

Robinson, W. A., 1991: The dynamics of low-frequency variability in a simple model of the global atmosphere. *J. Atmos. Sci.*, **48**, 429–441, https://doi.org/10.1175/1520-0469(1991)048<0429:TDOLFV>2.0.CO;2.

——, 1996: Does eddy feedback sustain variability in the zonal index? *J. Atmos. Sci.*, **53**, 3556–3569, https://doi.org/10.1175/1520-0469(1996)053<3556:DEFSVI>2.0.CO;2.

——, 2000: A baroclinic mechanism for the eddy feedback on the zonal index. *J. Atmos. Sci.*, **57**, 415–422, https://doi.org/10.1175/1520-0469(2000)057<0415:ABMFTE>2.0.CO;2.

——, 2006: On the self-maintenance of midlatitude jets. *J. Atmos. Sci.*, **63**, 2109–2122, https://doi.org/10.1175/JAS3732.1.

Simmons, A. J., and B. J. Hoskins, 1978: The life cycles of some nonlinear baroclinic waves. *J. Atmos. Sci.*, **35**, 414–432, https://doi.org/10.1175/1520-0469(1978)035<0414:TLCOSN>2.0.CO;2.

——, J. M. Wallace, and G. W. Branstator, 1983: Barotropic wave propagation and instability, and atmospheric teleconnection patterns. *J. Atmos. Sci.*, **40**, 1363–1392, https://doi.org/10.1175/1520-0469(1983)040%3C1363:BWPAIA%3E2.0.CO;2.

Song, J., 2016: Understanding anomalous eddy vorticity forcing in North Atlantic Oscillation events. *J. Atmos. Sci.*, **73**, 2985–3007, https://doi.org/10.1175/JAS-D-15-0253.1.

Song, K., L. Tao, and Y. Yang, 2023: On the intensification of typhoon *Damrey* with the monsoon gyre. *Quart. J. Roy. Meteor. Soc.*, **149**, 588–607, https://doi.org/10.1002/qj.4425.

Sun, Y., G. Chen, and B. Tan, 2021: Formation and maintenance mechanisms of the Pacific-Japan pattern as an intraseasonal variability mode. *Climate Dyn.*, **57**, 2971–2994, https://doi.org/10.1007/s00382-021-05851-4.

Swanson, K. L., P. J. Kushner, and I. M. Held, 1997: Dynamics of barotropic storm tracks. *J. Atmos. Sci.*, **54**, 791–810, https://doi.org/10.1175/1520-0469(1997)054<0791:DOBST>2.0.CO;2.

Tanaka, S., K. Nishii, and H. Nakamura, 2016: Vertical structure and energetics of the western Pacific teleconnection pattern. *J. Climate*, **29**, 6597–6616, https://doi.org/10.1175/JCLI-D-15-0549.1.

Uccellini, L. W., and P. J. Kocin, 1987: The interaction of jet streak circulations during heavy snow events along the East Coast of the United States. *Wea. Forecasting*, **2**, 289–308, https://doi.org/10.1175/1520-0434(1987)002<0289:TIOJSC>2.0.CO;2.

Ulbrich, U., and M. Christoph, 1999: A shift of the NAO and increasing storm track activity over Europe due to anthropogenic greenhouse gas forcing. *Climate Dyn.*, **15**, 551–559, https://doi.org/10.1007/s003820050299.

Uppala, S. M., and Coauthors, 2005: The ERA-40 re-analysis. *Quart. J. Roy. Meteor. Soc.*, **131**, 2961–3012, https://doi.org/10.1256/qj.04.176.

Wang, M., and B. Tan, 2021: Formation and maintenance mechanisms of the subseasonal eastern Pacific pattern: Energetics analysis. *Earth Space Sci.*, **8**, e2021EA001851, https://doi.org/10.1029/2021EA001851.

Xu, F., and X. San Liang, 2017: On the generation and maintenance of the 2012/13 sudden stratospheric warming. *J. Atmos. Sci.*, **74**, 3209–3228, https://doi.org/10.1175/JAS-D-17-0002.1.

——, and ——, 2020: The synchronization between the zonal jet stream and temperature anomalies leads to an extremely freezing North America in January 2019. *Geophys. Res. Lett.*, **47**, e2020GL089689, https://doi.org/10.1029/2020GL089689.

Yang, Y., R. H. Weisberg, Y. Liu, and X. San Liang, 2020: Instabilities and multiscale interactions underlying the loop current eddy shedding in the Gulf of Mexico. *J. Phys. Oceanogr.*, **50**, 1289–1317, https://doi.org/10.1175/JPO-D-19-0202.1.

——, J. C. McWilliams, X. San Liang, H. Zhang, R. H. Weisberg, Y. Liu, and D. Menemenlis, 2021: Spatial and temporal characteristics of the submesoscale energetics in the Gulf of Mexico. *J. Phys. Oceanogr.*, **51**, 475–489, https://doi.org/10.1175/JPO-D-20-0247.1.

——, X. San Liang, and W.-B. He, 2024: On the formation and maintenance of the interannual variability of the North Atlantic Oscillation, *J. Atmos. Sci.*, **81**, 177–208, https://doi.org/10.1175/JAS-D-23-0100.1.

Zhang, Y., X.-Q. Yang, Y. Nie, and G. Chen, 2012: Annular mode–like variation in a multilayer quasigeostrophic model. *J. Atmos. Sci.*, **69**, 2940–2958, https://doi.org/10.1175/JAS-D-11-0214.1.

Zhao, S., H.-L. Ren, F. Zhou, A. A. Scaife, and Y. Nie, 2023: Phase asymmetry in synoptic eddy feedbacks on the negatively-skewed winter NAO. *Atmos. Res.*, **288**, 106725, https://doi.org/10.1016/j.atmosres.2023.106725.

Zhao, Y.-B., X. San Liang, Z. Guan, and K. I. Hodges, 2019: The asymmetric eddy–background flow interaction in the North Pacific storm track. *Quart. J. Roy. Meteor. Soc.*, **145**, 575–596, https://doi.org/10.1002/qj.3453.

Zhuge, A., and B. Tan, 2021: The springtime western Pacific pattern: Its formation and maintenance mechanisms and climate impacts. *J. Climate*, **34**, 4913–4936, https://doi.org/10.1175/JCLI-D-20-0051.1.